Seventh International Conference on CFD in the Minerals and Process Industries
CSIRO, Melbourne, Australia
9-11 December 2009

EVALUATION OF TWO-EQUATION TURBULENCE MODELS IN A LABORATORY-SCALE THICKENER FEEDWELL

K. MOHANARANGAM, T. V. NGUYEN AND D. W. STEPHENS*

Parker Centre (CSIRO Minerals), Clayton, Victoria 3169, AUSTRALIA
*Darrin.Stephens@csiro.au

ABSTRACT

Single phase modelling studies have been carried out using commercially available software ANSYS-CFX (release 11.0) on a laboratory scale thickener feedwell geometry. With the increase in complexity of feedwell and thickener geometries, meshing with a hexahedral mesh is time-consuming and sometimes impossible. The first objective of this study is to test the effectiveness of using tetrahedral/prism meshes in thickener feedwell geometries. Experimental results from a previously published lab-scale thickener feedwell geometry has been compared against the numerical predictions to verify the accuracy of these meshes towards replicating the flow structure. Mesh independency studies were also carried with these tetrahedral/prism meshes. The second objective is to test the suitability of four currently available two-equation turbulence models in our thickener feedwell geometry and their resulting flow structure. These turbulence models have been tested for open feedwell geometries with and without a shelf.

NOMENCLATURE

a_1	SST *k-ω* turbulence model constant
B	body forces
$c_{r1\text{-}3}$	curvature correction constant
C_{scale}	curvature correction constant
$C_{\varepsilon 1\text{-}2}$	*k-ε* turbulence model constant
C_μ	*k-ε* turbulence model constant
D	rate of deformation
F_1	First SST blending function
F_2	Second SST blending function
f_r	modified streamline curvature strength
$f_{rotation}$	streamline curvature strength
k	turbulence kinetic energy
P_k	shear production of turbulence
P_{kb}	buoyancy production of turbulence
p	pressure
p'	modified pressure
r^*	curvature correction function
$\tilde{r}$	curvature correction function
S	strain rate
t	time
U	velocity
α_3	SST *k-ω* turbulence model constant
β'	SST *k-ω* turbulence model constant
β_3	SST *k-ω* turbulence model constant
ε	turbulence dissipation rate
μ	dynamic viscosity
μ_{eff}	effective viscosity
μ_t	turbulent viscosity
ρ	density
σ_k	*k-ε* turbulence model constant
σ_{k3}	SST *k-ω* turbulence model constant
σ_ε	*k-ε* turbulence model constant
$\sigma_{\omega 2}$	SST *k-ω* turbulence model constant
$\sigma_{\omega 3}$	SST *k-ω* turbulence model constant
υ_t	kinematic turbulent viscosity
Ω	vorticity
ω	turbulence frequency

Subscripts

i, j, k	velocity components

INTRODUCTION

Thickeners, as the name dictates, are used to concentrate fine particles from a slurry feed. Thickeners usually consist of a cylindrical feedwell surrounded concentrically by a large tank which forms the main body of the thickener. Slurry is fed into the feedwell along with a flocculant to induce the aggregation process under the turbulent conditions within the feedwell. Aggregates settle under gravity to produce a clear liquor collected from the outer edge of the upper surface of the thickener (overflow) and a concentrated underflow suspension of solids at the bottom of the tank. A slowly rotating rake is usually positioned at the base of the thickener to help move sediment out of the thickener for disposal or further processing. Industrial thickeners may be up to 100m in diameter, with feedwells up to 15m.

The feedwell is core to the overall operational performance of a thickener. Feedwell use as a flocculation reactor is a relatively recent innovation, with the introduction of synthetic polymer flocculants in the 1960s. Feedwells also aid in dissipating the kinetic energy of the feed stream, helping to achieve uniform settling with minimum turbulence, and thereby reducing/eliminating short-circuiting in the thickener.

Various mechanical aids like annular shelves may be installed within the feedwell to encourage an increase in kinetic energy dissipation from the inlet and also to enhance the residence time of the feed within the feedwell.

Previous flow measurement studies have been carried out in scaled down models of clarifiers/thickeners/settling tanks (Imam et al., 1983; Brestscher et al., 1992; Dahl et al., 1994; Zhou et al., 1994; Krebs et al., 1995; Moursi et al., 1995; Deininger et al., 1996; Larsen, 1997; Lakehal et al., 1999). Various mathematical models have also been developed within the framework of measured quantities. Most of the studies were 2D or 3D with more emphasis on the whole tank compared to the feedwell. However, Kahane et al. (2002) and Nguyen et al. (2006) did include the effect of feedwell in their CFD simulation of industrial scale thickeners.

White et al. (2003) showed that these physical investigations were generally focused on the fluid flow within the main body rather than the feedwell, not recognising the importance of the feedwell discussed above. Where feedwells have been considered, the techniques used to measure velocities had an error band of 20% or higher and the feedwell designs were usually oversimplified. Velocity measurements in more realistic feedwell geometries using laser based techniques were carried out by Sutalo et al. (2000, 2001) and White et al. (2003), wherein the associated errors were about 3%.

The same experimental data (White et al., 2003) is used in this current study to compare against the numerically predicted results. Two sets of data, one with and the other without a shelf within the feedwell, have been utilized in this study. The major aim is to compare these experimental results against the predicted values using tetrahedral/prism meshes and also to access the best turbulence model for the simulation of these feedwell thickener geometries.

MODEL DESCRIPTION

A single-phase numerical model was used to simulate flow in the small-scale thickener model. The model is based on the Reynolds Averaged Navier-Stokes equations using the eddy viscosity hypothesis:

Continuity Equation

$$\nabla \bullet \left(\rho \mathbf{U} \right) = 0 \tag{1}$$

Momentum Equation

$$\nabla \bullet \left(\rho \mathbf{U} \otimes \mathbf{U} \right) - \nabla \bullet \left(\mu_{eff} \nabla \mathbf{U} \right) = -\nabla p' + \nabla \bullet \left(\mu_{eff} \nabla \mathbf{U} \right)^T + \mathbf{B} \tag{2}$$

where **U** is the fluid velocity vector, ρ the fluid density, p' the modified pressure, μ_{eff} the effective viscosity and $\boldsymbol{B}$ is the body force.

The effective viscosity is given by

$$\mu_{eff} = \mu + \mu_t \tag{3}$$

Two-Equation Turbulence Models

Two-equation turbulence models are widely used in the CFD modelling of many industrial applications; they offer a good compromise between numerical effort and computational accuracy. They derive their name from the fact they solve both the velocity and length scales as two separate transport equations.

The *k-ε* and *k-ω* based two-equation models use the gradient hypothesis to relate the Reynolds stresses to the mean velocity gradients and the turbulent viscosity. The turbulent viscosity is defined as the product of a turbulent velocity and the turbulent length scale. In two-equation models, the turbulence velocity scale is generally computed from the turbulent kinetic energy obtained by the solution of a transport equation. The turbulent length scale is estimated from two properties of the turbulence field, usually the turbulent kinetic energy and either its dissipation rate or eddy frequency. The dissipation rate of the turbulent kinetic energy is provided from the solution of its transport equation.

k-ε Turbulence Model

Based on the above formulation, the values of *k* and ε are obtained by solving a differential transport equation and is given by equations (4) and (5), respectively

$$\nabla \bullet \left(\rho \mathbf{U} k \right) = \nabla \bullet \left[\left(\mu + \frac{\mu_t}{\sigma_k} \right) \nabla k \right] + P_k - \rho \varepsilon \tag{4}$$

$$\nabla \bullet \left(\rho \mathbf{U} \varepsilon \right) = \nabla \bullet \left[\left(\mu + \frac{\mu_t}{\sigma_\varepsilon} \right) \nabla \varepsilon \right] + \frac{\varepsilon}{k} \left(C_{\varepsilon 1} P_k - C_{\varepsilon 2} \rho \varepsilon \right) \tag{5}$$

The turbulent viscosity in equation (3) is computed using the formulation

$$\mu_t = C_\mu \rho \frac{k^2}{\varepsilon} \tag{6}$$

Here C_μ, $C_{\varepsilon 1}$, $C_{\varepsilon 2}$, σ_k and σ_ε are constants. P_k is the turbulence production due to viscous and buoyancy forces, which is modelled using

$$P_k = \mu_t \nabla \mathbf{U} \bullet \left(\nabla \mathbf{U} + \nabla \mathbf{U}^T \right) - \frac{2}{3} \nabla \bullet \mathbf{U} \left(3 \mu_t \nabla \bullet \mathbf{U} + \rho k \right) + P_{kb} \tag{7}$$

SST (Shear Stress Transport) Turbulence Model

The second two-equation turbulence model used in our current study is the *k-ω* based Shear-Stress-Transport (SST) model of Menter (1994). The transport equations for k and ω are given by equationns (8) and (9), respectively

$$\nabla \bullet \left(\rho \mathbf{U} k \right) = \nabla \bullet \left[\left(\mu + \frac{\mu_t}{\sigma_{k3}} \right) \nabla k \right] + P_k - \beta' \rho k \omega \tag{8}$$

$$\nabla \bullet \left(\rho \mathbf{U} \omega \right) = \nabla \bullet \left[\left(\mu + \frac{\mu_t}{\sigma_{\omega 3}} \right) \nabla \omega \right] + \left(1 - F_1 \right) \rho \frac{2}{\sigma_{\omega 2} \omega} \nabla k \nabla \omega + \alpha_3 \frac{\omega}{k} P_k - \beta_3 \rho \omega^2 \tag{9}$$

The combined *k-ε* and *k-ω* models do not account for the transport of the turbulent shear stress which results in an over-prediction of eddy-viscosity, and ultimately leads to a failed attempt in predicting the onset and the amount of flow separation from smooth surfaces. The proper transport behavior can be obtained by a limiter to the formulation of the eddy-viscosity and is given by

$$\nu_t = \frac{a_1 k}{\max\left(a_1 \omega, S F_2 \right)}; \quad \nu_t = \mu_t / \rho \tag{10}$$

Readers are advised that further information regarding the value of constants and blending functions can be found in the ANSYS-CFX (release11.0) manual.

SST with Curvature Correction

One of the weaknesses of the eddy-viscosity models is that they are insensitive to streamline curvature and system rotation, which play a significant role in many turbulent flows of practical interest. A modification of the turbulence production term is available to sensitize the standard eddy-viscosity models to these effects. So a

multiplier is introduced into the production term and is given by $P_k \rightarrow P_k f_r$, where

$$f_r = C_{scale} \max\{\min(f_{rotation}, 1.25), 0.0\} \quad (11)$$

The empirical functions suggested by Spalart and Shur (1997) to account for these effects are given by

$$f_{rotation} = (1 + c_{r1}) \frac{2r*}{1 + r*} \left[1 - c_{r3} \tan^{-1}(c_{r2} \tilde{r})\right] - c_{r1} \quad (12)$$

$$r* = \frac{\mathbf{S}}{\mathbf{\Omega}} \; ; \; \tilde{r} = \Omega_{ij}^{cc} \left(2\Omega_{ik} / \Omega_{mag}\right) / \mathbf{D}^{0.5} \quad (13)$$

$$\Omega_{ij}^{cc} = S_{jk} \left[\frac{DS_{ij}}{Dt} + \left(\varepsilon_{imn} S_{jn} + \varepsilon_{jmn} S_{in}\right)\right] \Omega_m^{rot} / \mathbf{D} \quad (14)$$

$$\Omega_{ij} = 0.5 \left[\left(\frac{\partial u_i}{\partial x_j} - \frac{\partial u_j}{\partial x_i}\right)\right] + 2\varepsilon_{mji} \Omega_m^{rot} \; ; \; \mathbf{D} = \max\left(\mathbf{S}^2, 0.09\omega^2\right) \quad (15)$$

$$\Omega^2 = 2\Omega_{ij}\Omega_{ij} \; ; \Omega_{mag} = \left(\Omega_{12}^2 + \Omega_{13}^2 + \Omega_{23}^2\right)^{0.5} ; S^2 = 2S_{ij}S_{ij} \quad (16)$$

In addition to the curvature correction within the SST model, a re-attachment option (proprietary to ANSYS CFX) within the SST model was also tested. Not much information could be found on how CFX handles it except for the inclusion of the term within the '*k*' equation as $P_{reattach}$.

EXPERIMENTAL APPARATUS AND TECHNIQUE

A short description of the experimental procedure is given here - for more information, refer White et al. (2003). The experimental apparatus consists of an optically transparent flat-bottomed thickener covered on the top with a transparent lid which housed both the feedwell as well as the central shaft. The feedwell models are 0.29m ID, 0.3m OD and 0.3m high. The annular shelf is 0.18m ID, 0.0145m high and the top of the shelf is located at 0.098m from the top of the feedwell. The central shaft is 0.032m OD and the feed pipe is 0.032 m ID. The annular drain in the base is 0.032m ID and 0.076m OD. An ONGA 112 pump was used to deliver water to the feedwell at flow rates of up to 120 L min^{-1}.

The LDV technique, which has been fully described by Durst et al. (1981), was used to measure the time-averaged velocity field and turbulence field in small-scale feedwell models on two vertical planes (perpendicular to each other) and two horizontal planes. The LDV system was operated in backscatter mode. To obtain 3D velocity information, measurements were taken from the side and top of the glass tank containing the open feedwell and thickener. A solid roof was necessary in the model to allow velocity measurements to be taken from the top. Initially, the velocity was measured in a few planes to determine an adequate sampling time and optimum LDV parameters. At test conditions, the inlet flow rate was ≈62 L min^{-1}, which corresponds to an average velocity of 1.285 ms^{-1} and a feed pipe Reynolds number of 38,000.

NUMERICAL PROCEDURE

The conservation equations of mass, momentum and turbulence given above were solved using a finite volume method in order to determine the single-phase liquid velocity for comparison against the experimental data. It is not possible to arrive at a solution with these equations using analytical approaches; thereby ANSYS-CFX (release 11.0) is used to solve them on unstructured grids. Rhie Chow (1983) interpolation is used to avoid chequer-board oscillations in the flow field. Coupling between velocity and pressure is handled implicitly by a coupled solver. Advection terms are discretized using the "High Resolution Scheme" which is second order accurate.

The turbulence models that were tested in this work have been outlined in Table 1. While studying the sensitivity of the various turbulence models, the solution of *k-ε* turbulence model was used as an initial guess for SST. The solution of SST turbulence model was used as an initial guess for SST with curvature correction and for SST with curvature correction & re-attachment modification. Standard wall functions within ANSYS CFX were used for *k-ε* turbulence model, while automatic wall functions were used for SST and its variants. In all simulations the y+ values were typically between 4- 40, however in certain areas (re-circulation) they were lower.

Table 1: Description of Simulations

Simulation No.	Turbulence Model
S1	*k-ε*
S2	SST
S3	SST + Curvature Correction
S4	SST + Curvature Correction + Re-attachment Modification

RESULTS

Grid independence studies on unstructured meshes for the feedwell both with and without a shelf were carried by varying the number of nodes from 100,000 to 750,000 (including the inflation). It was found that the solution no longer changes (i.e. plateaus) after 300,000 and therefore this was kept constant for studying the effect of turbulence models on the experimental data. The mesh distribution within the feedwell (with shelf) is shown in figure 1.

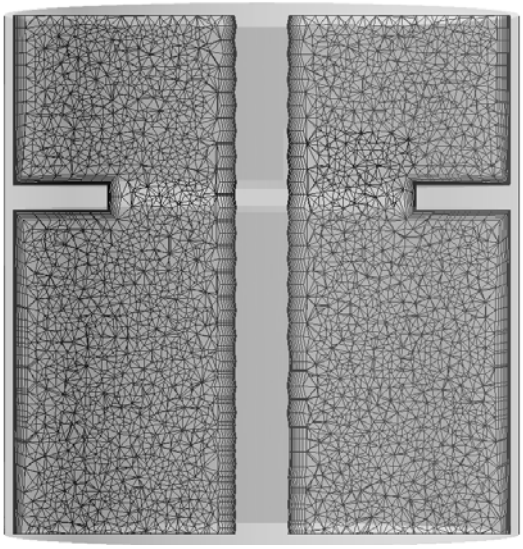

Figure: 1 Mesh distribution inside the Feedwell with the Shelf

No Shelf Configuration

In this section the numerical results are compared against the experimental data obtained by the LDV studies.

Figure 2 shows the comparison of experimental results with the predicted results for the no shelf configuration within the feedwell. The filled circles show the experimental data whereas the lines depict the predicted results. The left-hand side of the figure shows the comparison of tangential velocity results at a distance of 45mm from the top of the feedwell, whereas the right-hand side shows the axial velocity results at a distance of 290mm from the top of the feedwell.

The effect of using various two-equation turbulence models is quite evident from the figures. For tangential velocity profiles, experimental data depicts a symmetrical pattern along the centre of the feedwell and the shaft, with positive velocities along left side of the feedwell in the direction of the flow and negative velocities of flow circulation on the other half of the feedwell. The boundary layer along the shaft and the feedwell has been clearly resolved. The current two-equation turbulence models considered in our study will be used to test this feature of the flow as captured by LDV. The axial velocities or the upward/downward velocities along the shaft as depicted by LDV show that near the shaft the flow is directed downwards but as one moves from the shaft towards the walls of the feedwell the flow assumes a upward velocity and then a downward trend near the wall.

Simulation S1, which is the standard k-ε, does not seem to predict the boundary layer along the feedwell walls as well as the shaft; however, the magnitudes of the tangential velocities are in good agreement with the experimental data. This is not surprising, as the standard k-ε is very bad in capturing swirling flows (due to higher turbulence) as encountered around the feedwell and the shaft. For the axial velocities the predictions are quite in line with the experimental data, unlike the tangential velocity. The axial velocity does not experience a strong streamline curvature and hence the k-ε turbulence model is more suited to resolving this component of velocity. S2, which used the standard SST, shows a better prediction than S1 for both tangential and axial velocities. S3 shows the numerical results of SST with curvature correction and S4 shows the numerical results of SST with curvature correction and re-attachment option. While the tangential velocity shows a good comparison for simulations S3 and S4, the axial velocity does not, because the negative velocity magnitude is quite high near the proximity of the shaft.

With Shelf Configuration

Figure 3 shows the comparison of experimental and predicted results for the feedwell with a shelf. Two locations have been chosen for comparison. The left-hand side of the figure shows the comparison of tangential velocity results at a distance of 71mm from the top of the feedwell, whereas the right-hand side shows the axial velocity results at a distance of 290mm from the top of the feedwell. Experimental data for tangential velocities show almost a symmetrical pattern around the centre of the tank, however, the clear appearance of the boundary layer around the shaft and the feedwell is not quite as prominent as in the 'no shelf' configuration. This is due to the inherent presence of the shelf which seems to disturb the development of the boundary layer. Along these lines, the magnitude of the tangential velocities in the presence of a shelf is a lot higher than its counterpart. It can also be stated that the residence times of the flows with a shelf seem to be much higher than the 'no shelf' configuration, as the flow spirals over the top of the shelf before slipping from its edge into the inner wall of the feedwell.

S1 shows a good comparison for the tangential velocities whereas for the axial velocity there is an over-prediction from the numerical results. The SST model again shows a good comparison for the tangential velocities, whereas with respect to the axial velocities the predicted results are far better than S1, although a minor over-prediction is shown at the peaks. For S3 the predicted results are good for the tangential velocities whereas for the axial velocities a much flatter profile is predicted. From S4 it could be seen that overall, all the two-equation models are able to predict the tangential velocities accurately, whereas for the axial velocities S4 shows an over-prediction of the peak value.

CONCLUSIONS

Fluid flow in a model feedwell has been studied with the aid of a single-phase, three-dimensional CFD model. This study sought to ascertain whether the use of unstructured grids is valid for the study of thickener feedwells. A comprehensive mesh independence study was carried out. Various two-equation turbulence models have also been tested to ascertain the best model to replicate the fluid flow physics encountered in the feedwell. The results obtained have been compared against previous experimental data for both configurations of an open feedwell, i.e. with and without a shelf. It was concluded that tetrahedral/prism meshes can be used for the study of flow in feedwells. With respect to the choice of turbulence models, although k-ε turbulence model does produce similar results to the SST model, from a numerical and wall modelling/resolution point of view Shear Stress Turbulence (SST) model seem to be the best alternative.

ACKNOWLEDGEMENTS

The support of the Parker CRC for Integrated Hydrometallurgy Solutions (established and supported under the Australian Government's Cooperative Research Centres Program) is gratefully acknowledged.

REFERENCES

ANSYS-CFX release 11.0 Reference Manual

BRETSCHER, U., KREBS, P. and HAGER, W.H. (1992). "Improvement of flow in final settling tanks." *Journal of Environmental Engineering*, **118**, 307–321.

DAHL, C.P., LARSEN, T. and PETERSEN, O. (1994). ''Numerical modelling and measurement in a test secondary settling tank.'' *Water Science and Technology*, **30**, 219–228.

DEININGER, A., GÜNTHERT, F.W. and WILDERER, P.A. (1996). "The influence of currents on circular secondary clarifier performance and design", *Water Science and Technology*, 34, 405–412.

DURST, F., MELLING, A. and WHITELAW, J.H. (1981). "Principals and Practice of Laser-Doppler

Anemometry", second ed. Academic Press, New York, USA.

IMAM, E., McCORQUODALE, J.A. and BEWTRA, J.K. (1983). ''Numerical modelling of sedimentation tanks'', *Journal of Hydraulic Engineering*, **109**, 1740–1754.

KAHANE, R., NGUYEN, T. V. and SCHWARZ, M. P. (2002). "CFD modelling of thickeners at Worsley Alumina Pty Ltd", *Appl. Math. Modelling*, **26**, 281-296.

KREBS, P., VISCHER, D. and GUJER, W. (1995). "Inlet-structure design for final clarifiers". *Journal of Environmental Engineering* **121**, 558–564.

LAKEHAL, D., KREBS, P., KRIJGSMAN, J. and RODI, W. (1999). "Computing shear flow and sludge blanket in secondary clarifiers". *Journal of Hydraulic Engineering*, 125, 253-262.

LARSEN, P. (1977). "On the hydraulics of rectangular settling basins", *Report No.1001*, Department of Water Resource Engineering, Lund Institute of Technology, Lund, Sweden.

MENTER, F.R. (1994). ''Two-equation eddy-viscosity turbulence models for engineering applications'', *AIAA Journal*, **32**, 1598–1605.

MOUSRI, A.M., McCORQUODALE, J.A. and EL-SEBKHY, I.S. (1995). "Experimental studies of heavy radial density currents". *Journal of Environmental Engineering,* **121**, 920–929.

NGUYEN, T., HEATH, A. and WITT, P. (2006). Population balance-CFD modelling of fluid flow, solids distribution and flocculation in thickener feedwells. *5th International Conference on CFD in Process Industries, CSIRO*, 13th-15th December, Melbourne.

RHIE, C.M., and CHOW, W.L. (1983). "Numerical study of the turbulent flow past an airfoil with trailing edge separation", *AIAA Journal*, **21**, 1527-1532.

SPALART, P.R., and SHUR, M. (1997). "On the sensitization of turbulence models to rotation and curvature", *Aerospace Science and Technology,* **1(5)**, 297-302.

SUTALO, I.D., NGUYEN, T., and RUDMAN, M. (2000). "Modelling studies of fluid flow in a thickener feedwell model". *CHEMECA 2000*, Perth, Western Australia, 9–12 July.

SUTALO, I.D., NGUYEN, T., WHITE, R.B. and RUDMAN, M. (2001). ''Experimental and numerical investigations of the fluid flow in thickener feedwells'', *Sixth World Congress of Chemical Engineering*, Melbourne, Australia, 23–27 September 2001, paper 941.

WHITE, R.B., SUTALO, I.D. and NGUYEN, T. (2003). "Fluid flow in thickener feedwell models." *Minerals Engineering*, **16**, 145–150.

ZHOU, S., McCORQUODALE, J.A. and GODO, A.M. (1994). "Short circuiting and density interface in primary clarifiers", *Journal of Hydraulic Engineering*, **120,** 1060–1080.

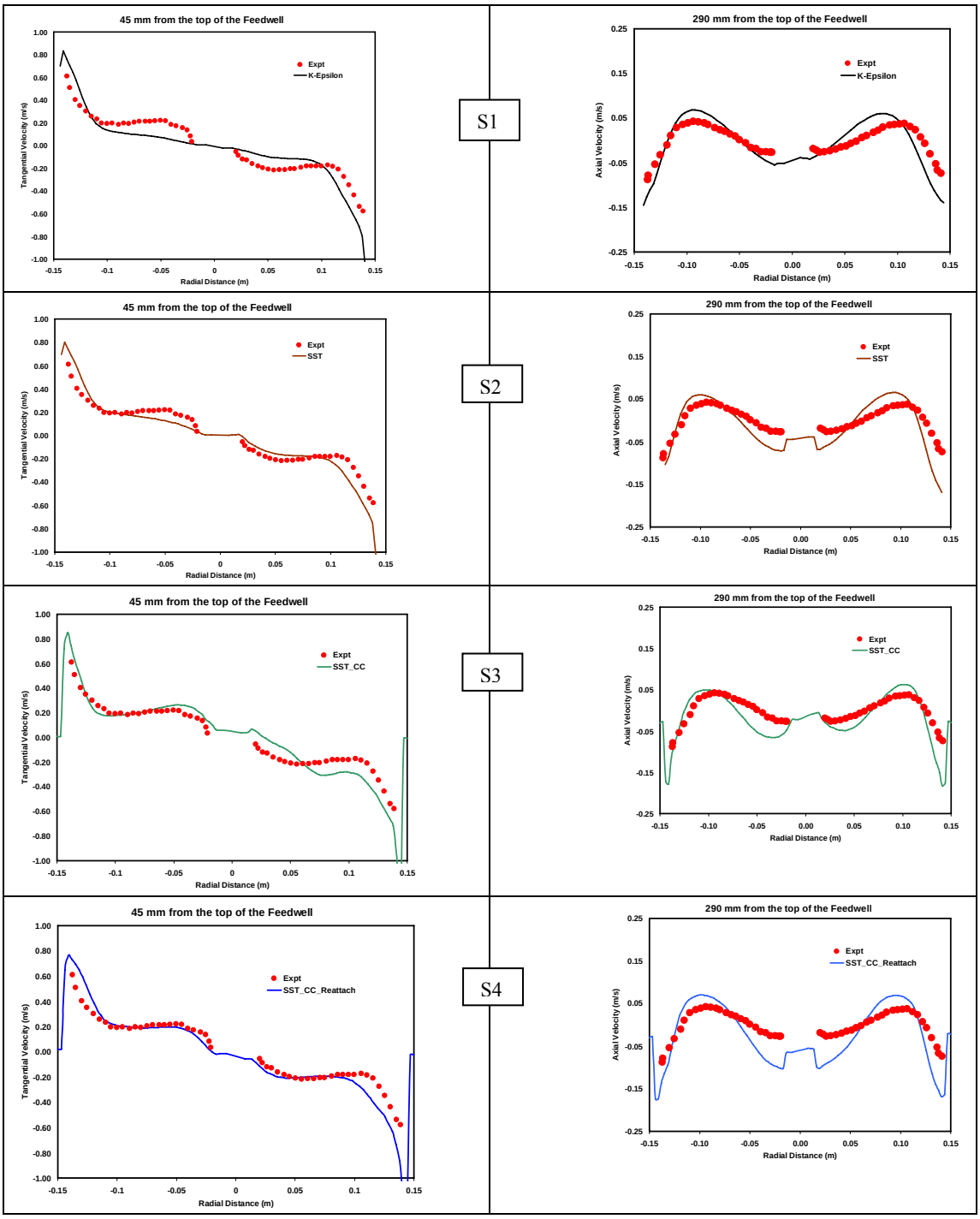

Figure 2: Comparison of predicted tangential and axial velocities with experimental data for the open feedwell with no shelf configuration

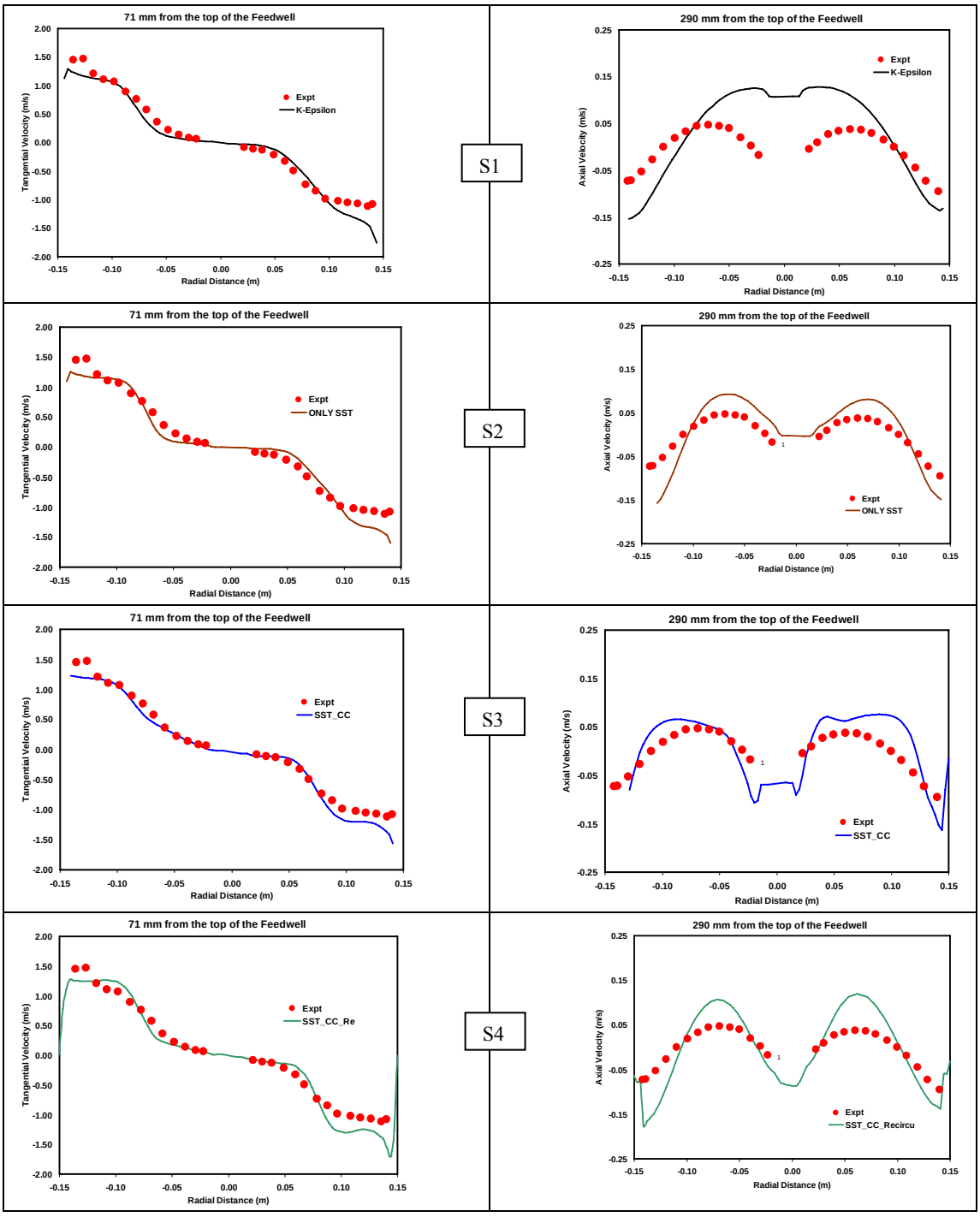

Figure 3: Comparison of predicted tangential and axial velocities with experimental data for the open feedwell with shelf configuration